Variable Carrier Phase Shift Method for Integrated Contactless Field Excitation System of Electrically Excited Synchronous Motors

Enes Ayaz, Ogün Altun, Ozan Keysan

Abstract—**This paper presents a novel contactless field excitation (CFE) system based on wireless power transfer (WPT), which utilizes the ~~already~~ existing voltage source inverter (VSI) of the motor ~~drives~~ drive for electrically excited synchronous motors (EESMs). In conventional CFE systems~~based on WPT~~, an extra high-frequency converter ~~next to the VSI of the motor drive is needed~~ is required to excite the field winding. ~~Unlike conventional systems~~In this paper, it is proposed ~~that the inherently existing voltage harmonic~~ to utilize existing voltage switching harmonics of the VSI ~~can be utilized to excite~~ for exciting the field winding while the low-frequency modulated component ~~still continues~~ is used to drive the motor. ~~However, the input excitation voltage of the WPT systemchanges by the modulation, which means that the motor operation affects the CFE system. Nonetheless, using only conventional control methods such as frequency detuning or post-regulation converters are unsuitable since they do not guarantee a continuous/constant power transfer under any motor operation. In this paper, a~~ To achieve the proposed system, a novel variable carrier ~~phase-shift~~ phase shift method (VCPSM) is ~~proposed~~ developed to achieve constant input excitation voltage for the WPT part independent of the motor operation. ~~Then, a mathematical model of the proposed VCPSM for sinusoidal pulse width modulation (SPWM) is developed, which can be easily implemented through online calculation. Further, a~~ In addition, a hybrid frequency detuning control method ~~, in addition to the VCPSM, is also~~ is introduced to adjust the field current finely. ~~Lastly, the mathematical model is validated experimentally, and the proposed CFE system is tested via a small-scale prototype. Thereby,~~ For experimental validation, a small-scale prototype with 100 V DC-link and 60 kHz switching frequency is established. It is observed that the field current could be kept almost constant at 5 A under different motor drive operations regarding modulation index and fundamental frequency by the proposed method. Also, it is beheld that the field current could be reduced by detuning the switching frequency. In brief, with only a software update and without an additional active converter, a cost-reduced and simple-to-implement ~~contactless field excitation system for electrically excited synchronous motors~~ CFE system for EESMs can be achieved using the proposed method.**

Index Terms—**Contactless field excitation, wireless power transfer, motor drive, SPWM, carrier phase shift**

I. Introduction

The ~~automotive industry opts for~~ interest of the automotive industry is continuously increasing in electric vehicles (EVs) or hybrid electric vehicles (HEVs) rather than internal combustion engine vehicles (ICEVs)~~since they have lower greenhouse gas emissions, which is vital to decelerate climate change~~ [1]. One of the critical parts of EVs and HEVs is the traction system, where ~~PM motors have usually been in high demand. PM motors usually provide high torque density and high efficiency compared to their alternatives, such as induction motors (IMs), switched reluctance motors (SRMs), and electrically excited synchronous motors (EESMs)~~ permanent magnet synchronous motors (PMSMs) are commonly preferred due to their high torque density [2]. However, ~~the~~ high cost and limited supply of rare-earth magnets such as Neodymium (Nd) and Samarium (Sm) encourage less-PM or no-PM motors such as ~~EESMs~~ electrically excited synchronous motors (EESMs) [3]–[6]. EESMs can decrease the total cost and ~~benefit from field-controlled regions~~ have flexible control thanks to their externally excited field windings [7], [8]. Moreover, they are more reliable as the demagnetization of PMs due to high temperature is not an issue in EESMs~~, increasing reliability~~. However, power transfer to their rotating field windings is challenging.

The most common method to excite field windings is to use slip rings ~~made up of~~ with conductor rings and carbon brushes. Although slip rings are a mature and cost-effective technology, they require periodic maintenance due to the wear of the brushes [9]. Another method is to use brushless exciters that are, in fact, synchronous generators (SGs) with rotating rectifiers. ~~This~~ However, this method is not applicable for variable speed drives such as in EVs [10]. Alternative to these methods, contactless field excitation (CFE) systems based on wireless power transfer (WPT) are proposed as shown in Fig. 1.a ~~–~~ [11]–[15]. They have no physical contact between the rotating and stationary frames, eliminating the maintenance issue. ~~Furthermore, their output power is independent of the motor speed, which makes them suitable for variable-speed motors. However, these systems increase~~ However, extra high-frequency converter increases the cost and complexity~~as they require extra high-frequency converters~~.

The ~~converter~~ VSI of the motor drive generates a low-frequency modulated voltage with high-frequency switching harmonics. This low-frequency modulated voltage controls the speed and torque of the motor, whereas the motor windings filter out the high-frequency voltage harmonics thanks to high phase inductances. In this paper, it is proposed that these high-frequency harmonics of the existing converter of the motor drive can be used to energize the ~~CFE system~~ field winding while the low-frequency modulated voltage can still be used to drive the motor. The proposed system is shown in Fig. 1.b.

Enes Ayaz, Ogün Altun, and Ozan Keysan are with the Department of Electrical and Electronics Engineering, Middle East Technical University, Ankara, Turkey

Corresponding Author: Ozan Keysan, keysan@metu.edu.tr

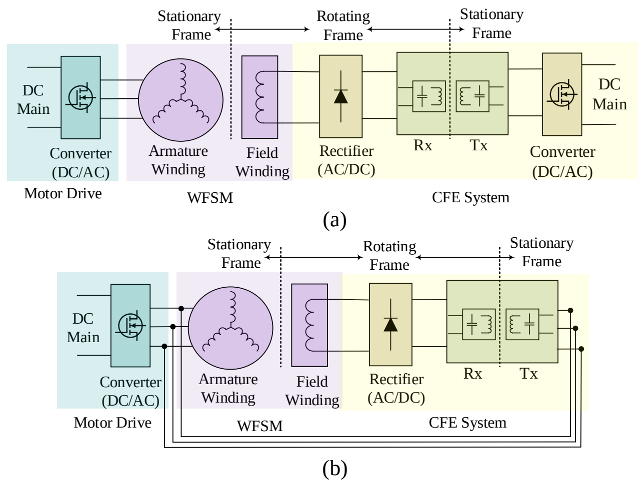

Fig. 1. The circuit diagram of a conventional and the proposed CFE based on a WPT system for EESMs. a) The conventional system. b) The proposed system.

~~Conventionally, motor drives utilize~~ Motor drives use modulation techniques such as sinusoidal pulse width modulation (SPWM) ~~and~~ or space-vector pulse width modulation (SVPWM). Yet, these modulation techniques affect the content of the high-frequency switching ~~harmonic components~~ harmonics in addition to controlling the low-frequency modulated voltage. Therefore, an independent control algorithm for the high-frequency switching harmonic components is required. In this study, a novel variable carrier phase-shift method (VCPSM) is proposed to achieve independent field current ~~from the motoroperation. Besides, the frequency detuning control method is applied concurrently with the proposed method to adjust the field current finely. Accordingly, the proposed method~~ control while driving the motor. The main advantage of the proposed method is that it can be applied in conventional motor drives by just ~~introducing control algorithms~~updating the software, so the system ~~'s cost and complexity can be reduced~~can be easily implemented without extra cost.

The rest of the paper is organized as follows. Section II presents the system structure and defines the problem. Section III proposes the variable carrier phase shift method and control strategy of the field current. Section IV gives the WPT system's design stage regarding the proposed method's restriction. Section ~~gives experimental resultsto validate the proposed system~~V presents the experimental results.

II. System Structure and Problem Definition

The proposed system ~~becomes prominent to achieve~~ aims for an integrated contactless field excitation system for electrically excited synchronous motors of EVs. A 2-level voltage source inverter (VSI) ~~in commercial EV drives~~ is the most common topology ~~.~~ in commercial EV drives [16]. In the past, discrete IGBTs or module IGBTs have been used ~~. Their switching frequencies are around 20kHz due to the switching losses~~ with their switching frequencies around 20 kHz [17]. Since the wireless power transfer systems become bulky in this frequency range, the proposed integrated CFE system is not feasible.

~~In~~ However, in recent years, wide band-gap semiconductors such as SiC MOSFETs or GaN HEMTs are becoming more popular in the automotive industry [18]. Thanks to their high switching frequencies up to 100 kHz, ~~that shrinks~~ the passive components can be shrunk [19]. Similarly, a higher switching frequency reduces the size of the transmitter and receiver coils of the WPT system and makes the proposed integrated CFE system more feasible.

Several topologies, such as capacitive power transfer (CPT) and inductive power transfer (IPT), can be used in CFE systems [20]–[28]. ~~The~~ Reducing the size of the system is essential as the system should fit inside the motor. Therefore, the IPT system is ~~suitable there~~ chosen thanks to its wide range of frequency, power, and smaller size. In IPT systems, Tx and Rx coils are loosely coupled, resulting in inherently low power factors. Therefore, compensation circuits are generally used [29]–[31]. Series compensation is preferred in the Tx coil as a VSI is used in motor drives. Besides, the Rx side compensation is not used since achieving a lightweight and small volume on the rotating side is desired in the proposed system.

In the remaining parts of the paper, a series-none (SN) topology is selected, and a 2-level 3-phase 3-wire (3Φ-3W) VSI (driven by SPWM) is used, although the proposed system can be adapted to different converters, modulation techniques, or WPT systems.

A. Problem Definition

Conventional WPT systems have two wire inputs, and motor drives have 3-wire outputs so that the WPT system can be connected between any two of three ~~wires~~phases, as given in Fig. 2.

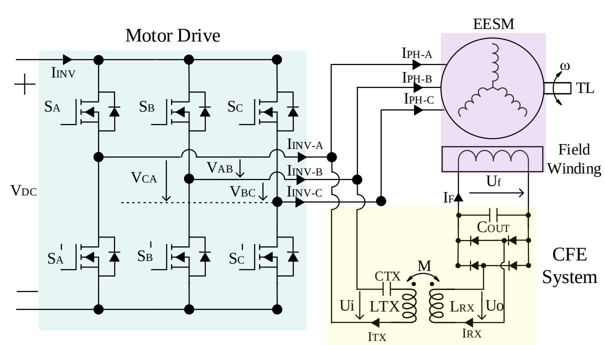

Fig. 2. The circuit diagram of the proposed system.

In this configuration (the WPT system will be connected between legs A and B), the excitation voltage of the WPT system (U_i) can be calculated as ~~given~~ in (1)

$$U_i = V_{DC} S_{AB} = V_{DC}(S_A - S_B) \tag{1}$$

where the switching function is calculated by double Fourier series as in (2) for SPWM.

$$
\begin{aligned}
S = {} & \frac{1}{2} + \frac{m_a}{2}\cos\Big(\omega_o t + \theta_o\Big) \\
& + \frac{2}{\pi}\sum_{i=1}^{i=\infty} J_o\Big(i\frac{\pi}{2}m_a\Big)\sin\Big(i\frac{\pi}{2}\Big)\cos\Big(i(\omega_c t + \phi_c)\Big) \\
& + \frac{2}{\pi}\sum_{i=1}^{i=\infty}\sum_{k=-\infty}^{k=\infty}\left(\begin{array}{c} \frac{1}{i}J_k\Big(i\frac{\pi}{2}m_a\Big)\sin\Big((i+k)\frac{pi}{2}\Big) \\ \cos\Big(i(w_c t + \phi_c) + k(w_o t + \theta_o)\Big)\end{array}\right)
\end{aligned}
\tag{2}
$$

~~As WPT systems behave like a bandpass filter characteristic,~~ There are four main components in SPWM for each leg: DC, fundamental, switching harmonics, and sidebands. However, only the first switching harmonic and its sideband components (denoted by U_i^f) ~~are utilized~~dominate in the WPT system since the WPT system behaves like a bandpass filter characteristic, and its resonant is tuned to near the switching frequency. Therefore, only U_i^f can be ~~calculated as~~ used in the mathematical model. U_i^f is given in (3), which is calculated by taking $(i = 1)$, $(i = 1, k = -2)$, and $(i = 1, k = 2)$ in (2)~~as a function of modulation index~~.

In conventional SPWM, each phase uses the same carrier signals. Hence, according to (3), the switching frequency disappears in U_i^f, and just only its sidebands exist. U_i and U_i^f are plotted in Fig. 3 for different modulation indices. It is observed that U_i^f increases with the modulation index, and zero voltage (zero excitation) occurs at some moments.

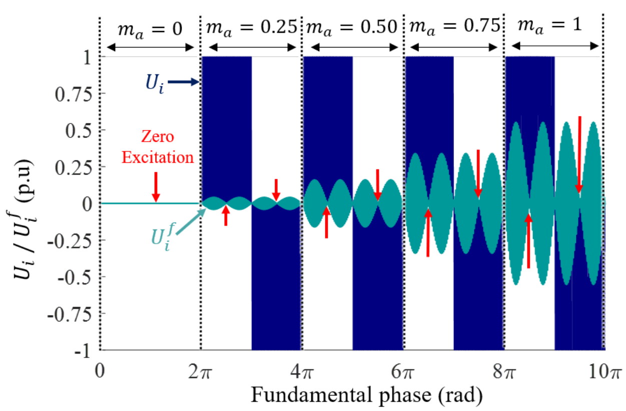

Fig. 3. The normalized input excitation voltage waveforms of the WPT system. Zero voltage points at input excitation voltage are indicated by red arrows.

Therefore, a control method is required to achieve a continuous/constant power transfer at the switching harmonic for the WPT system without disturbing the fundamental component. However, conventional control methods of the WPT system are not suitable for ~~achieving~~ this. A conventional method is ~~duty cycle control~~to control the duty cycle, but this also affects the fundamental component. Another method is frequency detuning control, but it cannot guarantee continuous power transfer since zero voltage moments exist, indicated via red arrows in Fig. 3. The last method is to add a post-regulation converter or use an active rectifier ~~. Nevertheless~~at the output of the WPT system. However, this increases the system's cost and complexity, and the problem of zero voltage ~~moment~~ moments still exists. ~~According to all above~~In this paper, a new control method~~should be developed~~ , introducing variable carrier phase shift, is proposed to avoid zero voltage moments and achieve continuous power transfer for changing modulation indices.

The proposed ~~system~~ method is similar to a dual-frequency power ~~transfers using~~ transfer system with a single converter [32]–[36]. In [33], a single-inverter-based dual-frequency WPT system is proposed using the programmed PWM method. However, the programmed PWM method is computationally complex and requires switching angle calculations using offline algorithms, which is not feasible in dynamic systems such as our cases. In [34], [35], multi-frequencies are achieved by comparing superimposed sinusoidal reference signals with a high-frequency triangular carrier ~~signals~~signal. However, in these methods, the switching frequency is higher than the operating frequencies of the WPT system, which increases the switching losses. In [36], multi-frequency components are achieved by a multi-level inverter (MLI) with a switching frequency lower than its two-level alternatives. However, this system uses a higher number of switching components, which is actually the opposite of the main proposal. In [37], a carrier-phase shift (CPS) method is proposed to control the switching harmonic independently. The amount of the CPS is determined according to the modulation index. Since a constant CPS is applied until the modulation index changes, a low-frequency ripple exist there.

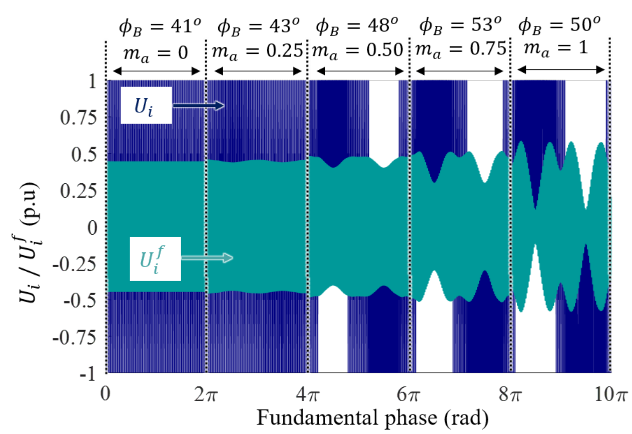

Fig. 4. The normalized input excitation voltage waveforms of the WPT system.

The low-frequency fluctuation is seen in Fig. 3. Although the low-frequency fluctuation may be acceptable in rotating loads and can be reduced by increasing the output capacitance, it should be mitigated in the application of the field excitation system since it also creates a torque and speed ripple in the motor. In order to solve this problem, the variable carrier phase shift method (VCPSM) is proposed.

This method calculates and updates the carrier phase shift for each duty cycle change rather than ~~the modulation change~~updating the modulation.

$$\frac{U_i^f(m_a)}{V_{DC}} = \frac{2}{\pi}J_2\left(m_a\frac{\pi}{2}\right)cos(2\pi(f_s-2f_o)t+\phi_A-2\theta_A) - \frac{2}{\pi}J_2\left(m_a\frac{\pi}{2}\right)cos(2\pi(f_s-2f_o)t+\phi_B-2\theta_B) + \frac{2}{\pi}J_2\left(m_a\frac{\pi}{2}\right)cos(2\pi(f_s)t+\phi_A)$$
$$-\frac{2}{\pi}J_2\left(m_a\frac{\pi}{2}\right)cos(2\pi(f_s)t+\phi_B) + \frac{2}{\pi}J_2\left(m_a\frac{\pi}{2}\right)cos(2\pi(f_s+2f_o)t+\phi_A+2\theta_A) - \frac{2}{\pi}J_2\left(m_a\frac{\pi}{2}\right)cos(2\pi(f_s+2f_o)t+\phi_B+2\theta_B) \tag{3}$$

III. The Proposed Variable Carrier Phase Shift Method (VCPSM) and Field Current Regulation

The variable carrier phase shift method aims to achieve a constant switching harmonic during each switching interval. In this section, firstly, a mathematical model is developed for SPWM. Then, the selection of the magnitude of the switching component is discussed. Finally, the regulation strategy of the field current is ~~examined~~presented.

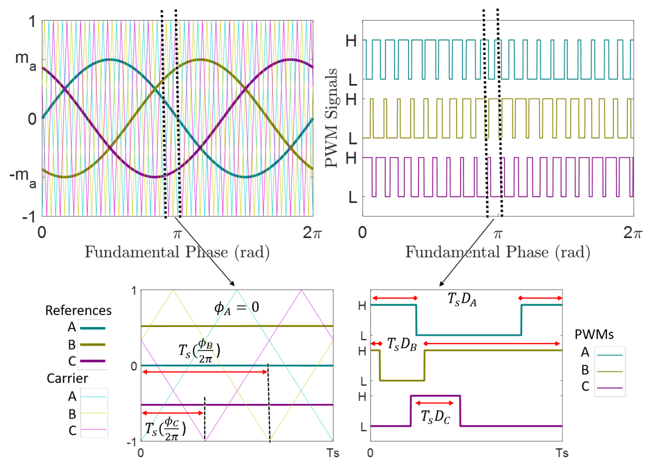

Fig. 5. The key waveforms of SPWM. For visual clarity, the switching frequency is decreased.

A. Mathematical Modelling

An example of SPWM with reference, carrier, and PWM signals is shown in Fig. 5 where different carrier signals are used for each phase. Here, the switching harmonic can be calculated as presented in (4) where ϕ_A, ϕ_B, and ϕ_C are the carrier phase angles.

$$\begin{aligned} S_A(t)^{f_s} &= \frac{2}{\pi}sin(\pi D_A)cos(2\pi f_s t+\phi_A) \\ S_B(t)^{f_s} &= \frac{2}{\pi}sin(\pi D_B)cos(2\pi f_s t+\phi_B) \\ S_C(t)^{f_s} &= \frac{2}{\pi}sin(\pi D_C)cos(2\pi f_s t+\phi_C) \end{aligned} \tag{4}$$

The normalized magnitude of the switching component for the phase-to-phase connection is calculated as ~~given~~ in (5).

$$\begin{aligned} S_{AB}(t)^{f_s} &= S_A(t)^{f_s} - S_B(t)^{f_s} \\ &= \frac{2}{\pi}sin(\pi D_A)cos(2\pi f_s t+\phi_A) \\ &\quad - \frac{2}{\pi}sin(\pi D_B)cos(2\pi f_s t+\phi_B) \end{aligned} \tag{5}$$

A phasor operation is required to calculate the peak value of the switching harmonic. ~~Considering~~ Utilizing (5), it ~~is calculated as given~~ can be calculated as in (6).

$$\hat{S}_{AB_{f_s}} = \frac{2}{\pi}\sqrt{\begin{array}{c} sin(\pi D_A)^2 + sin(\pi D_B)^2 \\ -2(sin(\pi D_A)(sin(\pi D_B)cos(\phi_A-\phi_B) \end{array}} \tag{6}$$

Thus, the magnitude of the switching component can be adjusted by ~~the~~ introducing a phase shift between the carrier signals. The required carrier-phase-shift value to keep $\hat{S}_{AB_{f_s}}$ constant at the desired value can be calculated using (5), and found as given in (7).

$$\phi_{CPS} = \phi_A - \phi_B = cos^{-1}\left[\frac{sin(\pi D_A)^2 + sin(\pi D_B)^2 - (\frac{\pi}{2}\hat{S}_{AB_{f_s}})^2}{2sin(\pi D_A)sin(\pi D_B)}\right] \tag{7}$$

The amount of carrier phase shift is restricted between 0^o and 180^o, which gives minimum and maximum $\hat{S}_{AB_{f_s}}$. Besides, D_A and D_B are not independent variables, and they follow the reference signals. Therefore, the reachable $\hat{S}_{AB_{f_s}}$ is restricted and ~~alters~~ changes regarding D_A, D_B, and ϕ_{CPS}. For these reasons, the selection of $\hat{S}_{AB_{f_s}}$ that is independent of the modulation index is challenging.

B. Selection of $\hat{S}_{AB_{f_s}}$

The maximum and minimum values of $\hat{S}_{AB_{f_s}}$ should be complied by triangle inequality, as given in (8).

$$\begin{aligned} \frac{2}{\pi}|sin(\pi D_A) - sin(\pi D_B)| &< \hat{S}_{AB_{f_s}} \\ &< \frac{2}{\pi}|sin(\pi D_A) + sin(\pi D_B)| \end{aligned} \tag{8}$$

Hence, these maximum and minimum values change according to modulation indices, as shown in Fig. 6. The aim is to

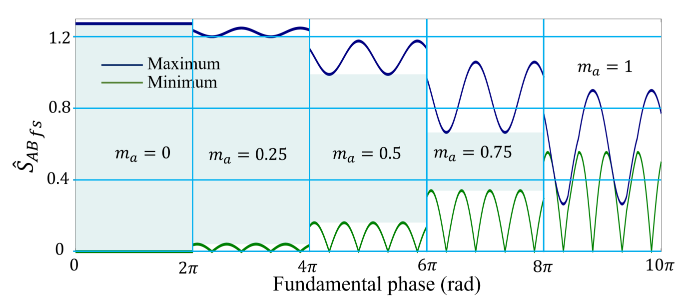

Fig. 6. The minimum and maximum normalized input excitation voltage limits for the proposed method under several modulation indices. The reachable excitation voltages are indicated by turquoise.

achieve a constant $\hat{S}_{AB_{f_s}}$ for any motor operation. However, it is observed that the range of the allowed $\hat{S}_{AB_{f_s}}$ is reduced by increasing the modulation index, and it may not guarantee a constant value for a higher modulation index. The allowed $\hat{S}_{AB_{f_s}}$ values are plotted along modulation indices in Fig.7.

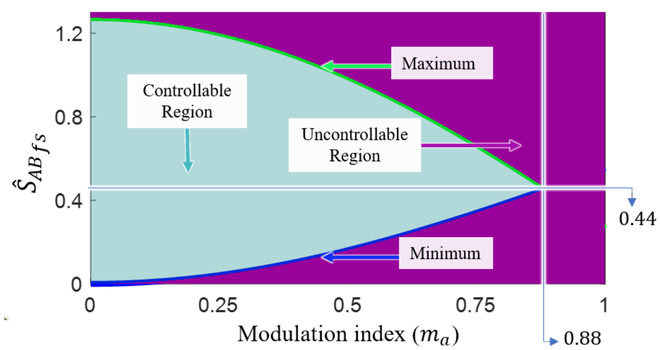

Fig. 7. Controllable and uncontrollable regions of the proposed method regarding modulation index.

The allowed range ~~becomes wide if the~~ of the WPT system is inversely proportional to the range of the motor drive control~~range could be narrow~~. For example, $\hat{S}_{AB_{f_s}}$ can be controlled between 0.30 and 0.60 for the modulation index below 0.6. Therefore, if a higher $\hat{S}_{AB_{f_s}}$ is desired, the modulation index of the motor drive should be restricted to a lower value, which also decreases the DC-link utilization. However, the selection of $\hat{S}_{AB_{f_s}}$, DC-link voltage, and modulation index are related to the system requirements. In this study, as a proof of concept, the $\hat{S}_{AB_{f_s}}$ limit is selected at 0.44, ~~and~~ where the motor operation ~~is~~ should be restricted to a maximum modulation index of 0.8.

C. Field Current Regulation

In the proposed method, the power of the WPT system is not ~~fully~~ directly controlled, but it only guarantees to keep the input excitation voltage at a constant value. Therefore, a control strategy for the field current should be developed. Several conventional methods are used in WPT systems, such as duty cycle control ~~,~~ and post-regulation converter (or active rectifier)~~, and frequency detuning control~~. The duty cycle control is ~~not suitable~~ unsuitable for cooperating with the proposed method since it also changes the fundamental component. ~~Although a~~ A post-regulation converter could be used, but it is not preferred as it increases the cost and complexity of the system. Alternatively, the frequency detuning method that controls the gain of the WPT system can be used, which does not require extra hardware and is simple to implement, so it is preferred in the proposed system. Accordingly, the overall control block diagram of the hybrid control strategy consisting of frequency detuning and variable carrier phase shift methods is presented in Fig. 8.

Firstly, the motor controller decides ~~duty cycles considering~~ the duty cycle according to the speed and torque references. Then, the CFE controller calculates the amount of carrier phase shifts by using these duty cycles; hence it keeps the

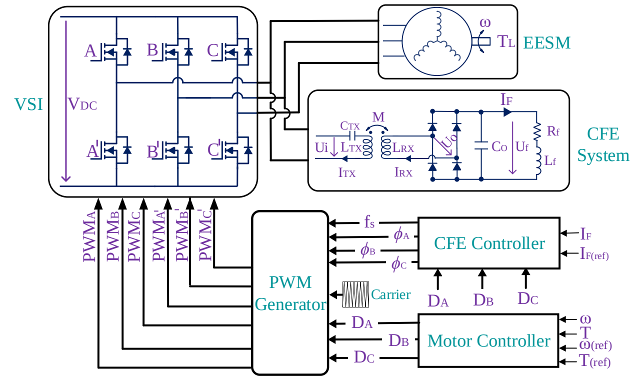

Fig. 8. The control schemes of the proposed CFE system.

input excitation to the desired value. Lastly, the CFE controller determines the switching frequency, ~~so it adjusts~~ which controls the gain of the WPT system, so the field current can be controlled accordingly.

IV. The Design of the WPT System

In this section, the design steps of the series-none (SN) compensated WPT system will be ~~given, considering the motor drive specifications~~presented. SN topology can be modeled by ideal transformer, leakage, and magnetizing inductances ~~. The simplified modeling without parasities~~ using the first harmonic approximation (FHA) ~~is~~ as shown in Fig. 9.

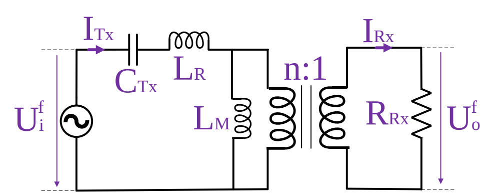

Fig. 9. The first harmonic approximation circuit diagram of the WPT system.

The load of the WPT system is the field winding of the EESM~~. The resistance~~ , and due to the field winding having high inductance, the field current is filtered out inherently. In the FHA model, to refer to the resistance of the input of the rectifier, only field resistance can be considered; in other words, the field inductance can be ignored, In this case, the resistance (R_{Rx}) and its voltage (U_o) can be found as given in (9) and (10) where R_F is the ~~field resistance~~ resistance of the field winding and U_F is the ~~field voltage~~ applied voltage of the field winding.

$$U_o = \frac{2\sqrt{2}}{\pi} U_F \tag{9}$$

$$R_{RX} = \frac{8}{\pi^2} R_F \tag{10}$$

Then, the transformer turns ratio can be calculated using the voltage gain as ~~given~~ in (11) where $U_i = \hat{S}_{AB_{f_s}} V_{DC}$.

$$n = \frac{U_i}{U_o} \tag{11}$$

The turns ratio depends on the Tx/Rx inductances and coupling factor (k) between them, presented in (12) where $L_{Tx} = \frac{L_R}{1-k^2}$.

$$n = k\sqrt{\frac{L_{Tx}}{L_{Rx}}} \tag{12}$$

The Rx inductance (L_{Rx}) is selected using the quality factor (Q), R_{Rx} and resonant angular frequency (ω_r), as given in (13).

$$L_{Rx} = Q\frac{R_{Rx}}{\omega_r} \tag{13}$$

ω_r is selected considering the switching frequency of the motor drive, as given in (14).

$$\omega_r = 2\pi f_s \tag{14}$$

Then, the Tx inductance is calculated using the required n, selected k, and L_{Rx}, as presented in (15).

$$L_{Tx} = \frac{n^2}{k^2}L_{Rx} \tag{15}$$

After that, the Tx compensation capacitance (C_{Tx}) is tuned as given in (16).

$$C_{Tx} = \frac{1}{\sqrt{\omega_r^2 L_R}} \tag{16}$$

~~Upon calculations above, the designed parameters of~~

V. Experimental Validation

An experimental setup consisting of a GaN-based 3ϕ-3W inverter and an SN-WPT-based CFE system is established, as shown in Fig. 10.

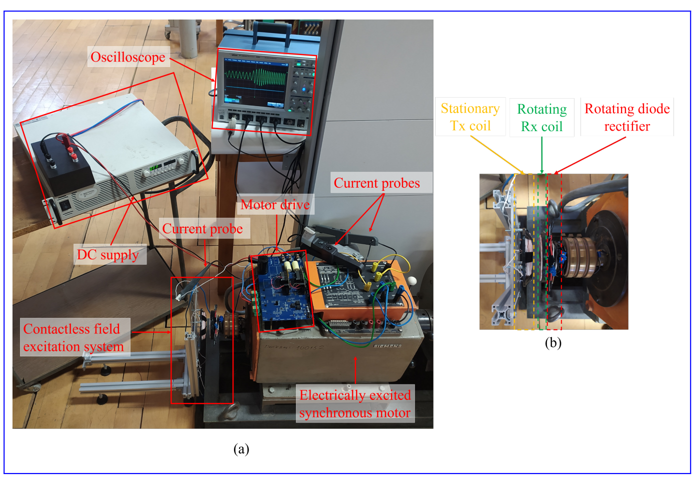

Fig. 10. Experimental setup. a) Overall view. b) Close view of the CFE system.

Table I presents the ~~SN-WPT system regarding the~~ motor drive ~~and field winding parameters are shown in Table I.~~ specifications, field winding specifications, and WPT system parameters.

~~Experimental setup.~~

TABLE I
THE MOTOR DRIVE ~~AND~~ SPECIFICATIONS, FIELD WINDING SPECIFICATIONS ~~OF~~ AND THE ~~THE~~ WPT SYSTEM PARAMETERS

Motor Drive Specifications	
DC-link Voltage (V_{DC})	100 V
Modulation Index (m_a)	$0 - 0.8$
Normalized input voltage ($\hat{S}_{AB_{f_s}}$)	0.44
Switching frequency (f_s)	~~65 kHz~~ 60 kHz
Field Winding Specifications	
Field Inductance (L_F)	5 mH
Field Resistance (R_F)	1.2 Ω
Field Current (I_F)	5 A
Field Voltage (U_F)	6 V
WPT System Parameters	**~~Designed~~ Experimental**
Tx Inductance (L_{Tx})	~~1500 μH 1500 μH~~ 1510 μH
Rx Inductance (L_{Rx})	~~6.5 μH 6.5 μH~~ 7.3 μH
Mutual Inductance (M)	~~48 μH 48 μH~~ 55.4 μH
Tx Capacitance (C_{Tx})	~~6.1 nF 6.1 nF~~ 5.2 nF

VI. ~~Experimental Validation~~

~~An experimental setup consisting of a GaN-based 3ϕ-3W inverter and an SN-WPT-based CFE system is established, as shown in Fig. 10. Table I presents the WPT system parameters.~~ Firstly, the proposed method is tested to validate the mathematical model. Secondly, the field excitation system is tested under several operating conditions of the fundamental frequency, modulation index, and switching frequency. Finally, the proposed CFE system is concurrently operated with the EESM.

A. Input Excitation Voltage of the VSI

The voltage waveform between phase A and phase B is measured while SPWM is applied in different modulation indices. ~~The DC-link voltage is 20 V, and the fundamental (reference) frequency is 100 Hz. The~~ The normalized voltage waveform and its decomposition of the switching harmonic are shown in Fig. ~~11~~ 11 for different modulation indices.

It is observed that a constant input excitation at 0.44 normalized gain is achieved until the modulation index of 0.8. The value starts fluctuating in higher modulation indices, after which is named the uncontrollable region. However, there is also a small fluctuation in the controllable region, and it can be ignored since it is under 5% of 0.44.

B. The Wireless Power Transfer System

The WPT system is connected between phase A and phase ~~B~~ B, like the previous test. The output of the WPT system is connected to the field of the EESM, but the phases of the EESM are not excited, which adds up to EESM not rotating. Firstly, the DC-link voltage and fundamental frequency are adjusted to 100 V and 100 Hz. The field current, Tx current, and input excitation voltage are measured for several modulation indices in the controllable region, as presented in Fig. ~~12. Thus, it is observed that a~~ 12. The mean currents of the field winding for the modulation index of 0, 0.25, 0.5, and 0.75 were measured at 4.83 A, 4.72 A, 4.95 A,

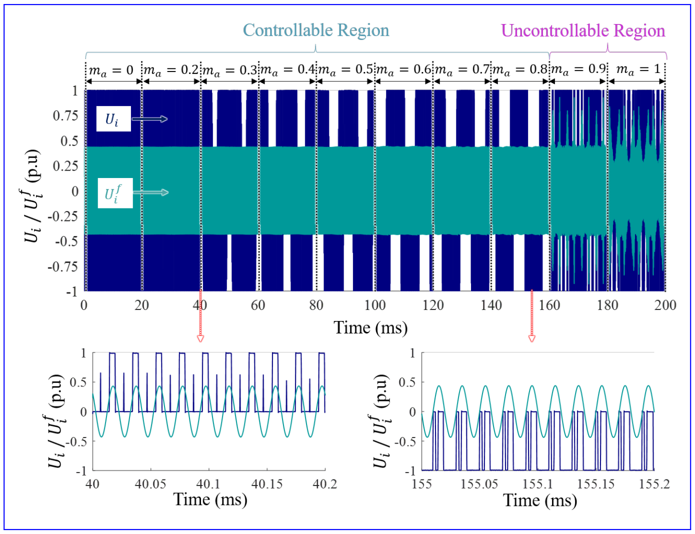

Fig. 11. The normalized voltage waveform of U_i and its decomposition of the switching frequency components U_i^f for different modulation indices.

and 4.93 A, respectively. Therefore, it is concluded that an almost constant field current can be achieved while changing the modulation index. These minor differences (maximum %5) can be compensated by detuning the switching frequency, which will be discussed thereafter.

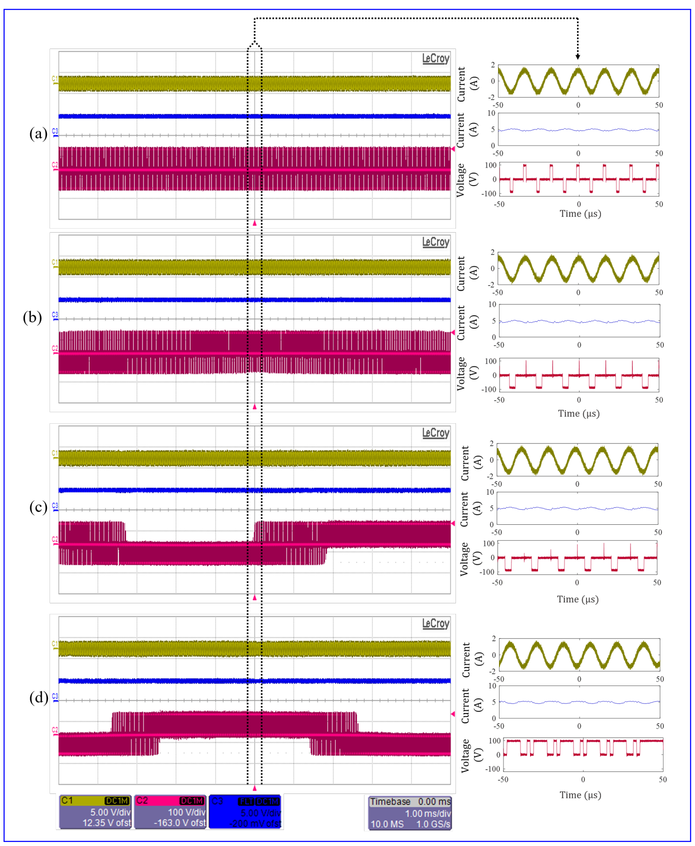

Fig. 12. The field current, Tx current, and input excitation voltage along several modulation indices under constant fundamental and switching frequency. a) $m_a = 0$. b) $m_a = 0.25$. c) $m_a = 0.5$. d) $m_a = 0.75$.

Secondly, the modulation index is kept at 0.6, and the fundamental frequency alters to ~~200 Hz from~~ 100 Hz from 200 Hz. The field current, Tx current, and input excitation voltage are given in Fig 13. Accordingly, it is monitored that the field current is not affected by the fundamental frequency. ~~The field current, Tx current, and input excitation voltage for fundamental frequencies of 100 Hz and 200 Hz under constant switching frequency and modulation index.~~

~~Finally~~Lastly, the modulation index and fundamental frequency are kept at 0.6 and 100 Hz. As presented in Fig. 14, the switching frequency is altered to ~~70 kHz from 65 kHz.~~ 60 kHz from 62 kHz. In this case, the field current decreases from 5 A to 2.5 A. Hence, it is achieved that the field current ~~is~~ could be regulated by the hybrid frequency detuning method.

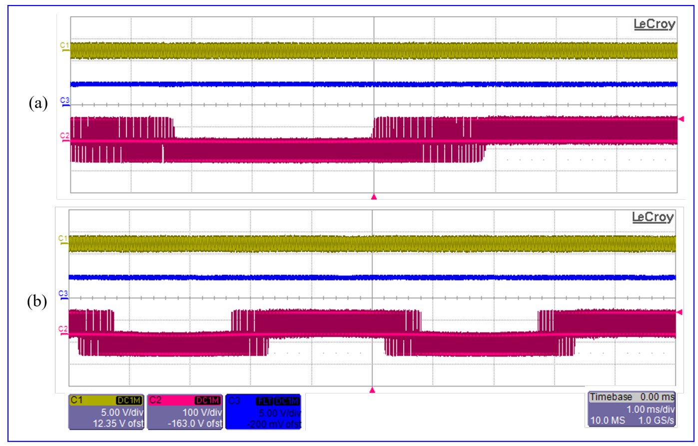

Fig. 13. The field current, Tx current, and input excitation voltage for ~~switching~~ fundamental frequencies of ~~65 kHz~~ 100 Hz and ~~70 kHz~~ 200 Hz under constant ~~fundamental~~ switching frequency and modulation index. a) 100 Hz. b) 200 Hz.

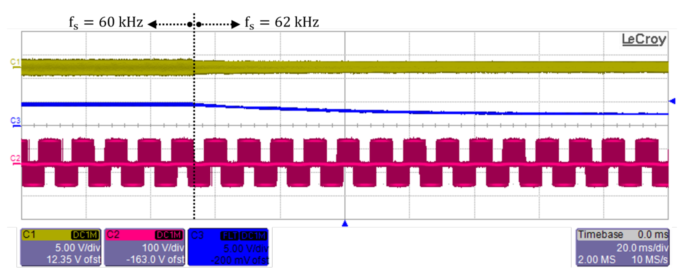

Fig. 14. The field current, Tx current, and input excitation voltage for switching frequencies of 60 kHz and 62 kHz under constant fundamental frequency and modulation index.

C. Concurrent Operation of the CFE System and EESM

In ~~the experimental prototype, the output of the WPT system is connected via a slip ring to take voltage measurements at the rotating output~~this test, the phases of the EESM are also excited in addition to the field winding. The speed of EESM is increased from ~~0 RPM to 500 RPM~~52 RPM to 101 RPM. The phase A current of the EESM and the field current are given in Fig. 15. Accordingly, it is observed that the ~~field current can be kept constant during varying motor speeds by the proposed method.~~ change in the motor speed minorly affects the field current. The minor changes can be compensated by detuning the switching frequency, as discussed before.

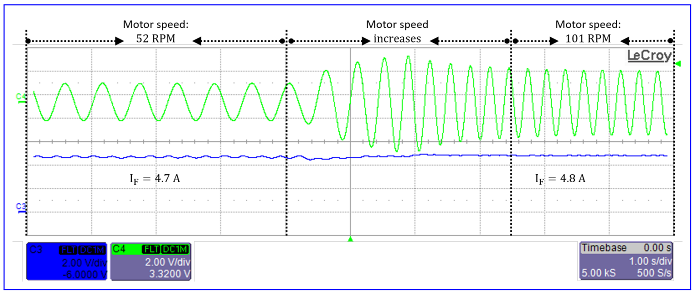

Fig. 15. The field and phase currents while ~~varying~~ motor ~~speeds~~speed increases from 52 RPM to 101 RPM.

VI. Conclusion

This article proposes a novel wireless power transfer-based contactless field excitation system that can be integrated into conventional electrically excited synchronous motors. Unlike traditional systems, the proposed method utilizes the existing motor drives and eliminates the ~~active converter on the Tx side~~requirement of extra converters on both the Tx and Rx sides, reducing the cost and complexity. This study also presents a novel variable carrier phase shift method for independent control of the field and phase current while using conventional PWM methods. However, the proposed method does not control the field current to the full range. It only guarantees a constant excitation voltage for different modulation indices. Therefore, a hybrid control strategy consisting of the VCPSM and frequency detuning methods is also presented to regulate field current. A prototype with a 3-phase GaN-based motor drive with 100 V DC-link and 60 kHz switching frequency was established to validate the proposed system. It is observed that the input excitation of the WPT system is kept constant at 44 V peak, which also means that the field current is kept almost constant at 5 A while changing the modulation index~~, and the results are coherent with analytical ones. It is also acquired~~. Also, it was achieved that the field current ~~can be regulated by the hybrid control method.~~ was reduced from 5 A to 2.5 A by detuning the switching frequency. Consequently, a cost-reduced CFE system for EESMs is achieved by only updating the control algorithm without using active converters.

References

[1] C. H. T. Lee, W. Hua, T. Long, C. Jiang, and L. V. Iyer, "A critical review of emerging technologies for electric and hybrid vehicles," *IEEE Open Journal of Vehicular Technology*, vol. 2, pp. 471–485, 2021.

[2] A. Naina, S. Paryani, and S. S. N. Jani, "Comparison between surface-mounted and interior pm motor for ev application," in *2021 International Conference on Intelligent Technologies (CONIT)*, 2021, pp. 1–6.

[3] H. Huang, Y.-S. Hu, Y. Xiao, and H. Lyu, "Research of parameters and antidemagnetization of rare-earth-less permanent magnet-assisted synchronous reluctance motor," *IEEE Transactions on Magnetics*, vol. 51, no. 11, pp. 1–4, 2015.

[4] D. G. Dorrell, "Are wound-rotor synchronous motors suitable for use in high efficiency torque-dense automotive drives?" in *IECON 2012 - 38th Annual Conference on IEEE Industrial Electronics Society*, 2012, pp. 4880–4885.

[5] I. Boldea, L. N. Tutelea, L. Parsa, and D. Dorrell, "Automotive electric propulsion systems with reduced or no permanent magnets: An overview," *IEEE Transactions on Industrial Electronics*, vol. 61, no. 10, pp. 5696–5711, 2014.

[6] F. Graffeo, S. Vaschetto, M. Cossale, M. Kerschbaumer, E. C. Bortoni, and A. Cavagnino, "Cylindrical wound-rotor synchronous machines for traction applications," in *2020 International Conference on Electrical Machines (ICEM)*, vol. 1, 2020, pp. 1736–1742.

[7] A. Di Gioia, I. P. Brown, Y. Nie, R. Knippel, D. C. Ludois, J. Dai, S. Hagen, and C. Alteheld, "Design and demonstration of a wound field synchronous machine for electric vehicle traction with brushless capacitive field excitation," *IEEE Transactions on Industry Applications*, vol. 54, no. 2, pp. 1390–1403, 2018.

[8] Y. Kim and K. Nam, "Copper-loss-minimizing field current control scheme for wound synchronous machines," *IEEE Transactions on Power Electronics*, vol. 32, no. 2, pp. 1335–1345, 2017.

[9] J. K. SkjØlberg, H. F. Ohma, and M. Runde, "Wear rates and current distribution of carbon brushes on steel slip rings," *IEEE Transactions on Energy Conversion*, vol. 24, no. 4, pp. 835–840, 2009.

[10] J. K. Nøland, F. Evestedt, J. J. Pérez-Loya, J. Abrahamsson, and U. Lundin, "Testing of active rectification topologies on a six-phase rotating brushless outer pole pm exciter," *IEEE Transactions on Energy Conversion*, vol. 33, no. 1, pp. 59–67, 2018.

[11] A. Di Gioia, I. P. Brown, Y. Nie, R. Knippel, D. C. Ludois, J. Dai, S. Hagen, and C. Alteheld, "Design of a wound field synchronous machine for electric vehicle traction with brushless capacitive field excitation," in *2016 IEEE Energy Conversion Congress and Exposition (ECCE)*, 2016, pp. 1–8.

[12] S. Hagen, M. Tisler, J. Dai, I. P. Brown, and D. C. Ludois, "Use of the rotating rectifier board as a capacitive power coupler for brushless wound field synchronous machines," *IEEE Journal of Emerging and Selected Topics in Power Electronics*, vol. 10, no. 1, pp. 170–183, 2022.

[13] J. Tang, Y. Liu, and N. Sharma, "Modeling and experimental verification of high-frequency inductive brushless exciter for electrically excited synchronous machines," *IEEE Transactions on Industry Applications*, vol. 55, no. 5, pp. 4613–4623, 2019.

[14] D. C. Ludois, J. K. Reed, and K. Hanson, "Capacitive power transfer for rotor field current in synchronous machines," *IEEE Transactions on Power Electronics*, vol. 27, no. 11, pp. 4638–4645, 2012.

[15] J. Dai, S. Hagen, D. C. Ludois, and I. P. Brown, "Synchronous generator brushless field excitation and voltage regulation via capacitive coupling through journal bearings," *IEEE Transactions on Industry Applications*, vol. 53, no. 4, pp. 3317–3326, 2017.

[16] A. M. Lulhe and T. N. Date, "A technology review paper for drives used in electrical vehicle (ev) hybrid electrical vehicles (hev)," in *2015 International Conference on Control, Instrumentation, Communication and Computational Technologies (ICCICCT)*, 2015, pp. 632–636.

[17] S. Tiwari, O.-M. Midtgård, and T. M. Undeland, "Sic mosfets for future motor drive applications," in *2016 18th European Conference on Power Electronics and Applications (EPE'16 ECCE Europe)*, 2016, pp. 1–10.

[18] B. Wrzecionko, D. Bortis, and J. W. Kolar, "A 120 °c ambient temperature forced air-cooled normally-off sic jfet automotive inverter system," *IEEE Transactions on Power Electronics*, vol. 29, no. 5, pp. 2345–2358, 2014.

[19] J. Millán, P. Godignon, X. Perpiñà, A. Pérez-Tomás, and J. Rebollo, "A survey of wide bandgap power semiconductor devices," *IEEE Transactions on Power Electronics*, vol. 29, no. 5, pp. 2155–2163, 2014.

[20] J. Dai, S. Hagen, D. C. Ludois, and I. P. Brown, "Synchronous generator brushless field excitation and voltage regulation via capacitive coupling through journal bearings," *IEEE Transactions on Industry Applications*, vol. 53, no. 4, pp. 3317–3326, 2017.

[21] D. C. Ludois, M. J. Erickson, and J. K. Reed, "Aerodynamic fluid bearings for translational and rotating capacitors in noncontact capacitive power transfer systems," *IEEE Transactions on Industry Applications*, vol. 50, no. 2, pp. 1025–1033, 2014.

[22] D. Maier, J. Kurz, and N. Parspour, "Contactless energy transfer for inductive electrically excited synchronous machines," in *2019 IEEE PELS Workshop on Emerging Technologies: Wireless Power Transfer (WoW)*, 2019, pp. 191–195.

[23] L. Sun, J. Kang, Y. Liu, Z. Mao, and Z. Zhong, "Wireless power transfer based contactless excitation of electrically excited synchronous motor," in *2020 IEEE 9th International Power Electronics and Motion Control Conference (IPEMC2020-ECCE Asia)*, 2020, pp. 1091–1097.

[24] X. Feng, Z. Fu, G. Hao, K. Wang, and Y. Weng, "Modeling and implementation of a new non-contact slip ring for wireless power transfer," in *2020 IEEE 9th International Power Electronics and Motion Control Conference (IPEMC2020-ECCE Asia)*, 2020, pp. 106–111.

[25] K. Song, B. Ma, G. Yang, J. Jiang, R. Wei, H. Zhang, and C. Zhu, “A rotation-lightweight wireless power transfer system for solar wing driving,” *IEEE Transactions on Power Electronics*, vol. 34, no. 9, pp. 8816–8830, 2019.

[26] R. Trevisan and A. Costanzo, “A 1-kw contactless energy transfer system based on a rotary transformer for sealing rollers,” *IEEE Transactions on Industrial Electronics*, vol. 61, no. 11, pp. 6337–6345, 2014.

[27] C. Zhang, D. Lin, and S. Y. R. Hui, “Ball-joint wireless power transfer systems,” *IEEE Transactions on Power Electronics*, vol. 33, no. 1, pp. 65–72, 2018.

[28] E. Ayaz, O. Altun, H. Polat, F. Karakaya, and O. Keysan, “Concurrent wireless power transfer and motor drive system with a single converter,” *IEEE Journal of Emerging and Selected Topics in Industrial Electronics*, pp. 1–9, 2022.

[29] X. Qu, H. Chu, S. C. Wong, and C. K. Tse, “An ipt battery charger with near unity power factor and load-independent constant output combating design constraints of input voltage and transformer parameters,” *IEEE Transactions on Power Electronics*, vol. 34, no. 8, pp. 7719–7727, 2019.

[30] X. Qu, H. Chu, S.-C. Wong, and C. K. Tse, “An ipt battery charger with near unity power factor and load-independent constant output combating design constraints of input voltage and transformer parameters,” *IEEE Transactions on Power Electronics*, vol. 34, no. 8, pp. 7719–7727, 2019.

[31] Y. H. Sohn, B. H. Choi, E. S. Lee, G. C. Lim, G.-H. Cho, and C. T. Rim, “General unified analyses of two-capacitor inductive power transfer systems: Equivalence of current-source ss and sp compensations,” *IEEE Transactions on Power Electronics*, vol. 30, no. 11, pp. 6030–6045, 2015.

[32] Z. Pantic, K. Lee, and S. M. Lukic, “Multifrequency inductive power transfer,” *IEEE Transactions on Power Electronics*, vol. 29, no. 11, pp. 5995–6005, 2014.

[33] C. Zhao and D. Costinett, “Gan-based dual-mode wireless power transfer using multifrequency programmed pulse width modulation,” *IEEE Transactions on Industrial Electronics*, vol. 64, no. 11, pp. 9165–9176, 2017.

[34] C. Xia, N. Wei, H. Zhang, S. Zhao, Z. Li, and Z. Liao, “Multifrequency and multiload mcr-wpt system using hybrid modulation waves spwm control method,” *IEEE Transactions on Power Electronics*, vol. 36, no. 11, pp. 12 400–12 412, 2021.

[35] J. Wu, L. Bie, W. Kong, P. Gao, and Y. Wang, “Multi-frequency multi-amplitude superposition modulation method with phase shift optimization for single inverter of wireless power transfer system,” *IEEE Transactions on Circuits and Systems I: Regular Papers*, vol. 68, no. 5, pp. 2271–2279, 2021.

[36] Y. Liu, C. Liu, X. Gao, and S. Liu, “Design and control of a decoupled multichannel wireless power transfer system based on multilevel inverters,” *IEEE Transactions on Power Electronics*, vol. 37, no. 8, pp. 10 045–10 060, 2022.

[37] E. Ayaz, O. Altun, and O. Keysan, “Carrier phase shift method of spwm for concurrent wired and wireless power transfer systems,” *IEEE Transactions on Industrial Electronics*, pp. 1–10, 2022.